1-Pa-7

超音波を用いたヒト関節軟骨音速測定値に軟骨変性度が与える影響についての検討

大橋 暁　大西 五三男　松本 卓也　別所 雅彦
戒田 健治　中村 耕三

【背景・目的】超音波による関節軟骨形態計測を行うためには軟骨音速の高精度測定が必要である．ヒト膝関節軟骨の音速を測定し，軟骨変性の程度が音速に及ぼす影響を検討した．

【方法】本研究における軟骨音速測定法は，第22回本学会で測定精度について報告したtime of flight法を用いた．倫理委員会の承認のもと，人工膝関節全置換術予定の変形性膝関節症患者より術前に同意を得た後，大腿骨顆部の骨軟骨切除片を収集した．患者数4名，検体数8，すべて女性で平均年齢は73.8±5.4歳であった．オリンパス社製の超音波送受信機(MODEL5800)と10 MHzのシングルプローブ(V 311-SU)を用い，脱気水(25℃)内で軟骨表面の3点においてRadiofrequency(RF)信号を検出した．信号はオシロスコープ(DPO4034, Tektronix)を介しコンピューターに記録し，軟骨表面境界，軟骨深層-石灰化軟骨境界(tidemark)に相当する各反射波の包絡線ピークを求め，peak-to-peak法により超音波飛翔時間(TOF: time of flight)を計測した．Minitom(Struers Inc.)を用い，信号検出点が断面を作成し，顕微鏡(MM-400, ニコン)により各点における軟骨表面からtidemarkまでの距離を軟骨厚として測定した．TOFおよび顕微鏡計測の軟骨厚より軟骨音速を算出した．音速測定後Safranin O-Fast Green染色による組織切片を作成，Mankin scoreにより軟骨変性評価を行い，音速測定値とMankin scoreについて回帰解析および相関解析を行った．

【結果】音速値の平均は1762.0±81.1 m/s，Mankinスコアと軟骨音速との一次回帰直線の式および相関係数の二乗はそれぞれ$y=-24.26\times+1877.2$，$R^2=0.2237$であった($p=0.251$)．Mankin scoreが高いほど軟骨の音速が減少する傾向にあった．

【考察】牛膝関節軟骨を用いた先行研究では，軟骨音速値は変性が進むほど低下すると報告されている(Toyras, et al. 2003)．今回，ヒト膝関節軟骨でも同様な結果が得られ，変形性膝関節症において関節軟骨形態計測を行うに際してこの点に留意する必要があると考える．

東大大学院整形

1-Pa-8

関節軟骨超音波評価法の誤差低減

山田 桂輔　山本 浩司　服部 祥治　富田 直

【緒言】近年，生体関節内で軟骨の状態を定量的に，軟骨に損傷を与えずに評価する方法として，超音波反を用いた関節軟骨定量評価法が開発されている．超音価法において軟骨変性の指標となる軟骨表面からの反の振幅は，超音波探査子の軟骨表面に対する照射角がでない場合大きく減少する．しかし，現在探査子の軟面に対する角度を推定する方法はない．臨床における関節の評価では，手作業で測定が行われるため，正確測するには時間を要するに多くの誤差を含みうる．究では，関節軟骨超音波評価法の精度向にのため，反の波形変化を用いた超音波探査子の反射面に対する角定を試みた．

【試料と方法】ステージに固定した軟骨(豚膝関節軟骨)ステンレス平板に対し超音波を照射し，反射波の振幅が大となるようにステージの角度を調節した．反射波の振が最大となる角度を0とし，そこから0.5ずつ5までステージを傾け，各角度における波形を測定した．測定は生理塩水中で行った．測定された反射波の波形の，1つ目のピークが計測されてから自由振動部の最初の負のピークが計されるまでの時間を，本研究ではPeak-to-Peak値と名づた．このPeak-to-Peak値を軟骨からの反射波とステンレからの反射波の各測定波形について計測し，探査子の傾との相関関係を調べた．

【結果と考察】探査子の角度とPeak-to-Peak値は正の相関を示した．このことから，測定波形からPeak-to-Peak値を計測することにより，探査子の傾きを推定できることが示唆された．また，Peak-to-Peak値の変化に対する反射強度の減少割合は，軟骨とステンレスで同じ傾向を示した．このことのから，Peak-to-Peak値を用いて反射波振幅の補正も可能であることが示唆された．

京大大学院工　奈良医大住医

81-1008　超音波による骨癒合強度定量評価の新しい計測システムの開発

宮坂　好一[1], 酒井　亮一[1], 鈴木　浩之[1], 大塚　利樹[1], 原田　烈光[1], 吉川　義博[1],
松山順太郎[2], 大西五三男[2], 中村　耕三[2]
[1]アロカ株式会社, [2]東京大学　医学部　整形外科教室

【はじめに】
骨癒合強度の評価において，現在のところ非侵襲で定量的かつ実用的な評価方法が確立されているとは言えない．我々は，超音波を用いて骨癒合度合いを非侵襲的かつ定量的に評価する計測方法を開発し報告してきた[1),2)]．今回は実用化を目指した新しい計測システムを開発したので，その内容と結果を報告する．

【方法】
超音波によるエコートラッキング（ET）法を用い，骨に荷重を与えたときに発生する骨表面の微小変位を計測することで骨の剛性を評価する．対象骨は脛骨である．被験者へ与える荷重値を低減するため，縦荷重から3点曲げ試験法による横荷重に改良した．その結果，荷重値を従来の約1/4に低減でき，より非侵襲性を高めた[3)]．これにともない評価指標をETS値[1)]から，屈曲角度ET－angle値[3)]に変更した（Fig.1）．
今回は特に，計測システムの実用化と小型化を目指し，新たなシステムを開発した．従来システムとの主な違いは次の点である．
(1) 9素子からなる探触子（Fig2左）を開発し，これを4つ用いた．
(2) 超音波の送受信チャネル数を4つに削減した．
(3) 開発した探触子を荷重点の両側に2つずつ配置し，ET計測点数を4点にした．
(4) パソコンベースにした．
なお，超音波の送信中心周波数は7.5MHzである．変位計測精度の評価は前回と同様に，水中で移動する金属平板の変位を接触式変位計（精度：1 μm）の値と比較した．

【結果】
変位計測精度は，接触式変位計の値に対し標準偏差が2.8 μmで，従来と同等であった．また，送受信チャネル数を減らしパソコンベースにしたことで計測システムを小型化できた（Fig.2右）．一方，Bモード画像の表示機能を省略したため，探触子の設定には慣れが必要であった．

【まとめ】
計測性能を維持したまま計測システムを小型化でき，実用性を高めた．

【参考文献】
1) 酒井，他，日超医抄録集，33(2006)，S501.
2) 酒井，他，日超医抄録集，34(2007)，S562.
3) R Sakai, et al, A Minute Bone Bending Angle Measuring Method using Echo-Tracking for Assessment of Bone Strength, IEEE Ultrasonics Sympo., pp.1116-1119, 2007.

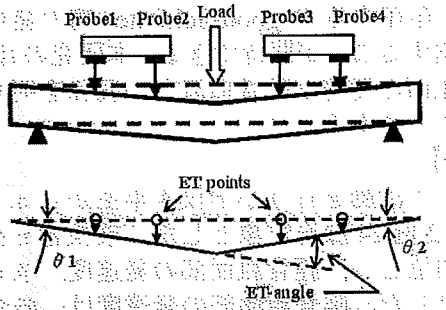

Fig.1　ET-angle値の説明図

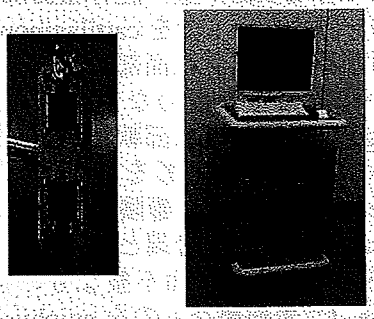
Fig.2 専用探触子(左)と計測システムの概観(右)

Development of a New Measurement System for Ultrasonic Quantitative Assessment of Mechanical Properties of Bone Healing

Koichi MIYASAKA[1], Ryoichi SAKAI[1], Hiroyuki SUZUKI[1], Toshiki OHTSUKA[1], Akimitsu HARADA[1], Yoshihiro YOSHIKAWA[1], Juntaro MATSUYAMA[2], Isao OHNISHI[2], Kozo NAKAMURA[2]
[1]ALOKA Co., Ltd., Tokyo, Japan,
[2]Department of Orthopaedic Surgery, Faculty of Medicine, University of Tokyo, Tokyo, Japan

A Minute Bone Bending Angle Measurement Method using Echo-Tracking for Assessment of Bone Strength In Vivo

R. Sakai[1], K. Miyasaka[1], E. Minagawa[1], T. Ohtsuka[1], A. Harada[1], Y. Yoshikawa[1], J. Matsuyama[2], K. Tobita[2], K. Nakamura[2], I. Ohnishi[2]

[1]Aloka Co.,Ltd., Tokyo, Japan

[2]Department of Orthopaedic Surgery, Faculty of Medicine, University of Tokyo, Tokyo, Japan

Abstract—**The purpose of this study is to develop a new ultrasound diagnostic system for non-invasive and quantitative assessment of mechanical properties of the bone or bone healing. In the previous papers [1] [2], we reported that we had developed a new ultrasound system to measure a minute bone deformation using a multi-point echo-tracking (ET) and that it had a great potential for non-invasive and quantitative diagnosis of bone healing. In this paper, we present a newly developed measurement system with improved accuracy for assessing deformation of intact tibia in vivo. It consists of a dedicated probe, a transmitting/receiving system and analysis software calculating a minute bending angle of the bone surface under a three-point bending (TPB) test. And, we report results of a performance evaluation of the developed system by using test measurements. Furthermore, we evaluated the reproducibility of the in vivo measurement by repeatedly measuring the bending angle of the tibias of 5 healthy volunteers every week for one month. As a result, the evaluation of the accuracy of the measured bending angle using the metallic plate for calibration showed that the standard deviation (SD) of the measurement in range of 0 to 0.1 degrees was 0.004 degrees. Then, we performed an in vivo measurement of normal tibia. The results showed that the mean bending angle of the normal adult tibias under a load of 25N and a supporting span of the tibial length of each subject was 0.058 degrees with a SD of 0.01 degrees. In addition, SD of the data for the measurement repeatability was 0.006 degrees. We developed a bending angle measurement system for the human tibia using a TPB test and obtained an excellent accuracy of the system and also confirmed through the measurement of the tibia of human volunteers that the repeatability was sufficient to quantitatively assess bending property of the intact tibia.**

Keywords:Echo-tracking;Non-invasive;Bone mechanical property

I. INTRODUCTION

In the treatment of fractures, the mechanical properties of the fracture healing site provide useful diagnostic information on the assessment of the degree of healing. Until now, it has been difficult to quantitatively assess the mechanical properties of the bone noninvasively. In clinical practice, the diagnosis of the bone healing has been performed by X-ray images. However, this evaluation is neither quantitative nor noninvasive resulting in re-fracture after union or non-union due to the lack of sufficient accuracy. To solve the problem, we have developed a method to quantitatively assess the mechanical property of the fracture site. The method utilizes ultrasound to measure the amount of a minute deformation of the bone subjected to a small load.

We validated the accuracy and clinical usefulness of the fracture healing assessment system which we developed by applying Echo-Tracking (ET) method [3] by measuring strain of a bone model and by applying the method to fracture patients. The results on the capability of quantitative evaluation of the process of bone healing have already been described [2]. In the bone model experiment, the correlation between the ET-strain (ETS) measurement and the strain measurement of the bone surface was very high. In vivo evaluation of fracture patients, the progress of the bone healing could be quantitatively assessed in all of the patients from the first stage of the consolidation period to the final stage. In the current study, we tried to improve the measurement accuracy and reproducibility to be able to expand the application to non-fractured bones with bone fragility such as osteoporosis. To this end, we enhanced the measurement accuracy of the system.

II. METHODS

We describe the new measurement algorithm that applied the three-point bending (TPB) test method, the newly developed measurement system and its evaluation method.

A. *Measurement algorithm*

To apply the TPB test method, we change the load direction from axial compression to bending. The measured item is the bending angle of the bone under the load. We can obtain sufficient deformation of the bone surface even under a smaller bending than that of axial compression. Moreover, as the load direction can be controlled, the direction of the deformation can be specified. Fig.1 shows the diagrams of the measurement method. In order to further improve the measurement accuracy, the bone surface displacement of the proximal and distal sides of the loading point is measured by using two probes. The

spacing of probes is 110mm. A water bag is put on the probe surface to eliminate the influence of the bone surface shape and to provide an acoustic coupling. Each probe is equipped with two transducers. The spacing of transducers is 40mm. These four transducers acquire the RF signals from each of the four points on the object surface by ultrasound transmitting and receiving. The total of four displacements of the object generated by the load are measured by analyzing the RF signals using the ET method. Thereafter, the two inclination angles of the proximal and distal bone surface are calculated from the four displacements, and finally the bending angle (ET-angle) of the object bone is obtained by adding these two inclination angles.

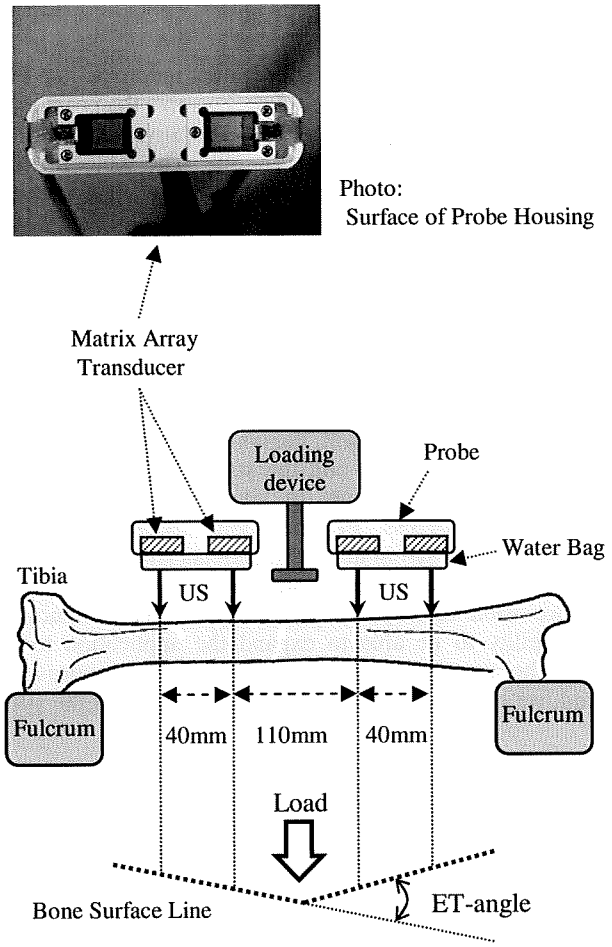

Fig.1 The principle of measurement method using TPB test method
The measured item is the bending angle of the bone under the load. The bone surface inclination on both sides of the load point is measured by using two probes. The ET-angle is calculated by adding each inclination angles obtained by two probes.

B. Measurement system

The measurement system consists of two ultrasound probes, transmitter and receiver, a computer controlled loading device to load the target bone, a leg-holder and a system control/data analysis software.

We developed a new dedicated ultrasound transducer of the matrix array format (3*3, pitch 3mm, 7.5MHz). The transducer is small and lightweight to be able to improve the positioning accuracy for the ET measurement, and to make the handling easier. The purpose of introducing a matrix array format is to identify measurement points easily for ET on the bone surface with various curvature. In addition, we also developed a dedicated ultrasound transmitter and receiver to enable the simultaneous four-point measurement with four matrix array transducers.

Previously, loading on the object bone had been performed with a human hand. To reduce the measurement error factor, we developed a computer controlled loading device. This device applies initial load of 5N to the object bone and, after a few seconds, increases the load up to 30N (maximum load). The reason to have a few seconds pause is to avoid the influence of the visco-elasticity of the soft tissue that might affect the results of the measurement. The loading rate can be arbitrarily specified. In this study, we set it at a speed of 4N/s that does not give uncomfortable feeling to volunteers.

The software of this system controls simultaneously the loading device and the ultrasound transmitter/receiver. The initial load of 5N is automatically applied when an examiner pushes the measurement start button, and then the ultrasound transmitter/receiver starts to operate automatically, and after a few seconds, the loading device starts to increase the load up to 30N. By off-line processing, the displacement of the bone is measured from acquired RF signals by the ET measurement method, and the ET-angle is obtained from the difference of displacements between the 5N and 30N loading. As the object bone is being covered with soft tissue, there is some overall sinking of the bone surface along the loading direction. However, the effect of this translation on the calculating angle can be removed by using differential measurement on the elements of array transducers.

For the measurement in vivo, we developed a U-shaped leg holder to support and stabilize the lower leg.

C. Evaluation of measurement accuracy

Fig.2 shows the diagram of the measurement setup. We measure an inclination angle of the surface polished metallic plate (SUS420J2, 270*60*5t mm, flatness variation 2μm less) tilted by a micrometer using our measurement system simultaneously with an optical displacement meter with an accuracy of 0.5μm (LK-G150, Keyence, Japan). Each inclination angle was calculated by the individually measured displacements and the spacing of the measured points using arctangent. The spacing of transducers is 40mm. The one of optical displacement is 100mm.

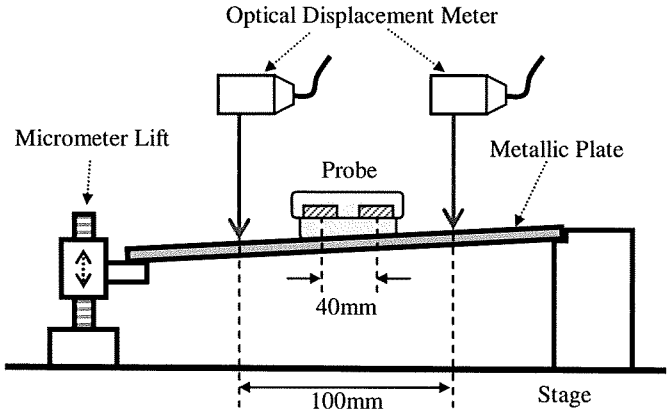

Fig.2 Evaluation method of inclination angle
The inclination of metallic plate measured with optical displacement meter and this system simultaneously. The inclination angle is calculated by each differential displacement and spacing of the measured points using arctangent. The spacing of transducers is 40mm. The one of optical displacement is 100mm. Each inclination angle is compared.

We evaluate the accuracy of the inclination angle measurement of our system by comparing with those of the optical displacement meter.

Next, we perform the ET-angle measurement by using the TPB test of a tibia bone model (SAWBONES 3rdGeneration Composite Tibia, Pacific Research Laboratories, Inc., USA) which simulated the elasticity of the human tibia. Because there is no soft tissues, due to the differential algorithm, the angle is estimated to be close to that measured in vivo. Fig.3 shows the photograph of measurement configuration.

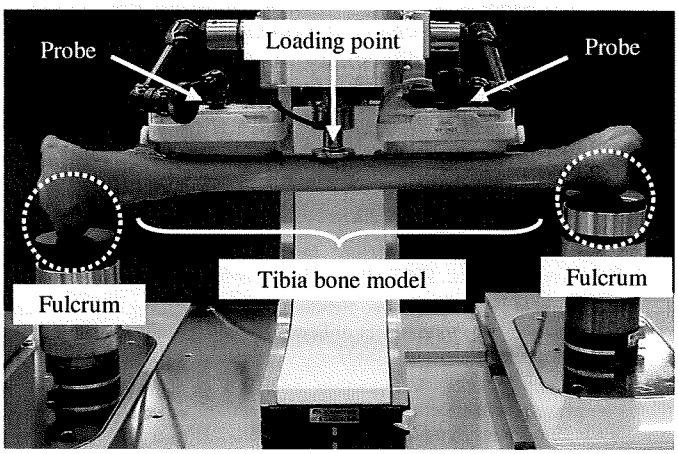

Fig.3 TPB measurements of tibiae bone model
Each end of the bone model is placed on a fulcrum (lower side of the figure). Loading point and two probes are arranged on the midline of the medial surface of tibia (upper side of the figure). The loading device applies the load and the angle is measured using the ET method.

D. Evaluation in vivo

For in vivo evaluation, the measurement area by ET is selected to be the medial surface of the tibia which is suitable for the ultrasound assessment. The proximal fulcrum is positioned at the head of the fibula, and the distal one at the lateral malleolus. These positions are selected because a) they can be easily found by palpation, b) they provide easy access through a thin layer of the soft tissue and c) they offer good balance and a comfortable position for volunteers. The U-shaped leg holder (width of the proximal: 60mm, width of the distal: 30mm) is developed in order to support the lower leg. A silicon sponge is attached to the surface of the leg holder, and the stability of the support was ensured. Loading point is adjusted and placed on the appropriate position on the medial side of the tibia, projected from the midpoint between the head of the fibula and the tip of the lateral malleolus measured on the opposite side. The direction of the load is vertically set to the measurement side. Fig.4 shows the photograph of measurement configuration.

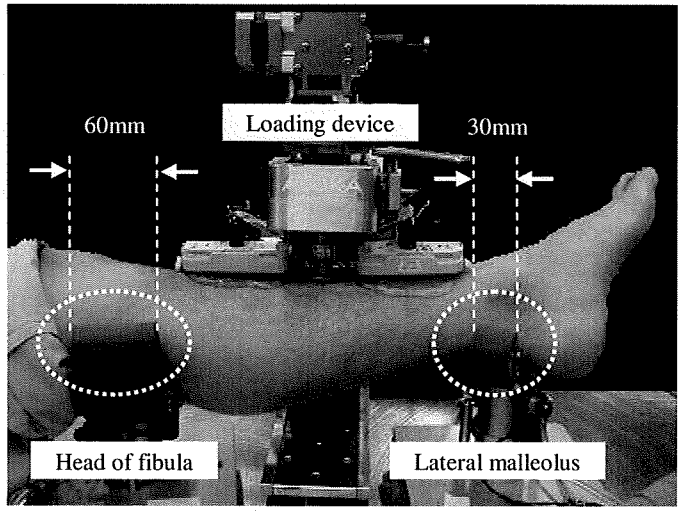

Fig.4 TPB measurements of human tibia
The lower leg is placed on the leg-holder. The proximal fulcrum is set at the level of the head of fibula. The distal one is at the lateral malleolus. The loading device and the probe are arranged on the midline on the medial surface of tibia side. The ultrasound signals from the tibial surface during loading are acquired.

E. Assessment of reproducibility in vivo

The reproducibility of the ET-angle measurement by this system is evaluated by in vivo evaluation method as previously mentioned. Each of the left tibia of five healthy volunteers (from ages 24 to 57) is evaluated four times every week. In each experiment, the measurement is repeated three times and the means and the standard deviations are calculated.

III. Results

The accuracy of the inclination angle measurement by this system was 0.004 degrees. Because the theoretical accuracy of the angle/displacement measurement with the ET method is 0.004 degrees ($\tan^{-1}$[3μm/40mm]), it could be confirmed that the accuracy of our system was extremely high almost equivalent to the theoretical value.

As the result of TPB measurement by using tibia bone model, the ET-angle of 0.073 degrees (0.003SD) was obtained under the load of 25N. These values are the mean and standard deviation of five times measurement results. Because the bone model has the elasticity equal with a human bone [4], we were able to estimate the order of ET-angle of the human tibia.

The result of TPB measurement and the reproducibility of the measurement of the human tibia are shown in Table 1 and Fig.5. The variation of each trial in ET-angle showed the reproducibility by assuming that the tibial property would not change during the measurement period. The mean of the standard deviation of the ET-angle measurement was 0.006 degrees in the whole persons. Considering the accuracy of the inclination measurement of this system was 0.004 degrees, this result showed high reproducibility.

Table 1 The reproducibility of the system in vivo every week

Subject	Sex	Age	Tibial length [mm]	Tibial width [mm]	ET-angle [degrees]	First week	Second week	Third week	Fourth week	Ave. /4weeks	SD /4weeks
E.M.	Male	57	330	32.0	Ave.	0.039	0.050	0.040	0.057	0.047	0.008
					SD	0.003	0.003	0.005	0.010		
R.S.	Male	35	320	28.9	Ave.	0.075	0.076	0.073	0.069	0.073	0.003
					SD	0.010	0.013	0.005	0.014		
K.H.	Male	36	330	38.3	Ave.	0.068	0.059	0.051	0.049	0.057	0.009
					SD	0.012	0.004	0.005	0.004		
N.I.	Male	24	340	40.4	Ave.	0.067	0.053	0.053	0.058	0.058	0.007
					SD	0.005	0.000	0.004	0.005		
H.S.	Male	42	334	36.0	Ave.	0.058	0.056	0.049	0.050	0.053	0.004
					SD	0.003	0.006	0.009	0.003		
										Ave. 0.058	0.006
										SD 0.010	

TPB test for the tibia are measured by load of 25N (5N→30N). The subjects are five volunteers (Age: 24-57). The evaluation method is to measure same person four times every week. In each experiment, the measurement is repeated three times and means and standard deviations are calculated.

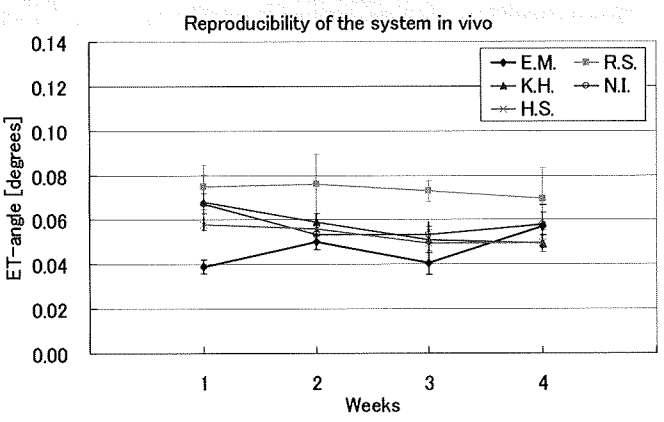

Fig.5 The reproducibility of the system in vivo every week
The mean and the standard deviation of ET-angle in each volunteer were plotted every week.

IV. Discussions and Conclusion

We developed a new measurement algorithm and system in order to evaluate the mechanical properties of human tibia with high accuracy and reproducibility. As a result, the possibility of evaluation for not only the fractured bone but also non-fractured bone with bone diseases such as osteoporosis was obtained.

References

[1] A.Harada et al., A New Method for Measuring Bone Strength using Echo-Tracking, Proc. IEEE Ultrasonics Symposium, pp.13-16, 2006

[2] R.Sakai et al., A Minute Bone Bending Angle Measuring Method using Echo-Tracking for Assessment of Bone Strength, Proc IEEE Ultrasonics Symposium, pp.1116-1119, 2007

[3] A.Harada, T.Okada, M.Sugawara and K.Niki, Development of a noninvasive real-time measurement system of wave intensity, Proc IEEE Ultrasonics Symposium, pp.1517-1520, 2000

[4] Luca Cristofolini, Marco Viceconti, Mechanical validation of whole bone composite tibia models, Journal of Biomechanics 33, pp.279-288, 2000

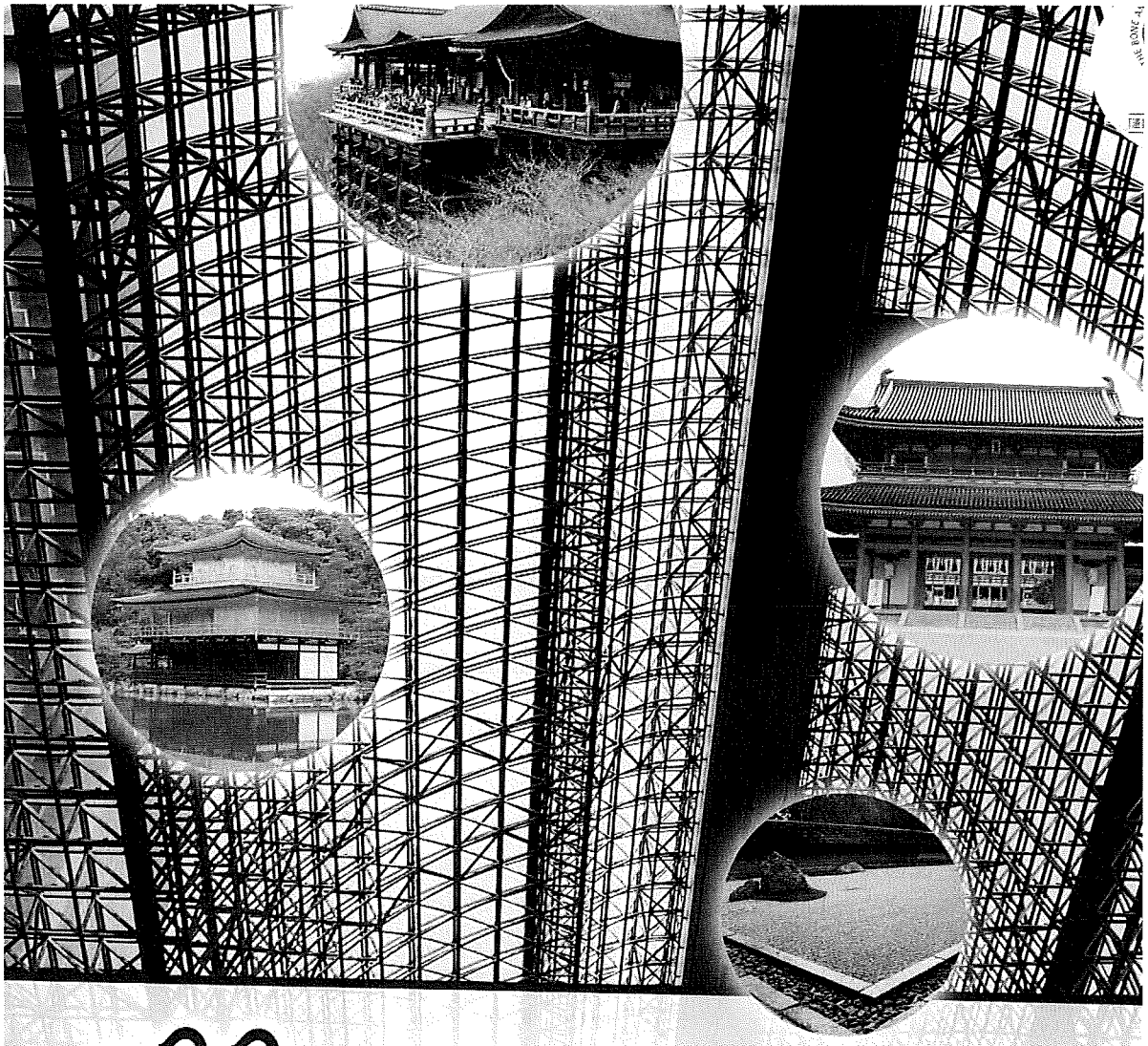

第22回
日本創外固定・骨延長学会

抄録集

会期　2009年3月6日(金)・7日(土)

会場　ウェスティン都ホテル京都

会長　久保　俊一（京都府立医科大学大学院 運動器機能再生外科学 教授）

1-PD1-06

超音波エコートラッキング法を用いた骨癒合の評価

○大西　五三男、松山　順太郎、飛田　健二、別所　雅彦、大橋　暁、松本　卓也、金子　雅子、中村　耕三

東大大学院整形

Quantitative Evaluation of Fracture Healing in vivo Using Ultrasound Echo Tracking

○ Isao Ohnishi, Juntaro Matsuyama, Kenji Tobita, Masahiko Bessho, Satoru Ohashi, Takuya Matsumoto, Masako Kaneko, Kozo Nakamura

Orthop. Surg., Graduate School of Medicine, The Univ. of Tokyo

【背景】骨癒合を評価するにあたりX線写真による定性的方法は骨の形状や荷重方向といった力学的情報が欠如しており正確とは言えない。骨癒合においては骨の力学強度の回復が重要であり骨の力学特性を評価することにより可能と言える。我々は体内の骨の歪を非侵襲に計測可能なエコートラッキング（ET）法を用いた新たな診断装置を開発した。ET法は超音波エコー信号の位相変化を測定するもので、荷重負荷に対する動的な骨の微小変形を2.6 μ mの精度で測定可能とした。この装置を用い、骨の力学特性であり骨強度と密接に関係する剛性測定を行い骨強度評価を行った。

【方法】脛骨骨折患者（保存療法：2名2肢、手術療法：12名14肢）を対象とし測定を行った。下腿の近位・遠位を固定し、骨折部近傍において25Nの曲げ荷重を加え、近位・遠位骨片の傾斜角（ET変形角）を測定した。測定は2～6週間隔で実施し、測定期間は平均21.2週で測定回数は平均6.1回であった。ET変形角の経時変化を健側肢と比較し骨癒合を定量評価した。

【結果】保存療法・手術療法のいずれの症例においてもレントゲン上、正常な骨癒合が進行した症例ではET変形角は経時的に指数関数的に減少し、骨癒合を定量評価可能であった。一方、手術症例でレントゲン上、仮骨の形態変化を示さない症例のET計測では、いずれも経時測定で明らかな減少はなく、骨癒合不全であることが診断可能であった。

【考察】ET計測によりin vivoにおいて非侵襲に骨癒合の進行と遷延が定量診断可能であった。今後、非侵襲に骨強度評価を行う方法として骨折の骨癒合評価だけでなく脆弱性を有する骨に対しても応用可能であると考える。

Available online at www.sciencedirect.com
ScienceDirect
ELSEVIER
Computerized Medical Imaging and Graphics 31 (2007) 643–655
Computerized Medical Imaging and Graphics
www.elsevier.com/locate/compmedimag

Hip cartilage thickness measurement accuracy improvement

Yuanzhi Cheng [a,b,c,*], Shuguo Wang [b], Takaharu Yamazaki [c,d], Jie Zhao [b], Yoshikazu Nakajima [e], Shinichi Tamura [c,d]

[a] *School of Computer Science and Technology, Harbin Institute of Technology in Weihai, China*
[b] *Mechareonic Engineering Department Robitics Institute, Harbin Institute of Technology, China*
[c] *Division of Image Analysis, Osaka University Graduate School of Medicine, Japan*
[d] *Center for Advanced Medical Engineering and Informatics, Osaka University, Japan*
[e] *Department of Bioengineering, School of Engineering, University of Tokyo, Japan*

Received 6 December 2005; received in revised form 27 July 2007; accepted 2 August 2007

Abstract

Accurate measurement of the distance separating two adjacent sheet structures, such as femoral cartilage and acetabular cartilage in the hip joint is important in evaluation of osteoarthritis. A new method, insensitive to the influence of adjacent sheet structures, was developed to improve the accuracy of hip cartilage thickness measurement. A theoretical simulation for investigating the influence of adjacent sheet structures on the accuracy of cartilage thickness measurement in MR images was performed. The thickness is defined as the distance between zero-crossings of the second directional derivatives along the sheet surface normal direction. The simulation measurement showed considerable underestimation in thickness measurement occurred due to the influence of the adjacent sheet. A new method based on a model of the MR imaging process to eliminate the influence of adjacent sheet structure was developed and tested using phantoms and two cadaveric human hip joint MR scans. The new method reduced the influence of the adjacent sheet structure was more accurate than the conventional method for measuring hip cartilage thickness.

Keywords: Cartilage thickness; Point spread function; Measurement accuracy; Theoretical simulation; Line filter responses; Second directional derivative; Zero-crossings

1. Introduction

Accurate thickness measurement of sheet-like (or plate-like) thin anatomical structures, such as articular cartilage, has become increasingly important in clinical applications. Osteoarthritis or posttraumatic articular injuries can result in changes to the morphology of articular cartilage. Measuring and monitoring changes of articular cartilage thickness can play a critical role in the management of patients with disease or injury to those tissues.

The majority of studies for measuring the articular cartilage thickness have focused on the knee joint [1–5], where the cartilage surfaces do not fit tightly. Only a limited number of studies have addressed cartilage abnormalities in the hip joint [6,7]. In the hip, both the femoral head and the acetabulum are covered with cartilage. The ball and socket constitution of the hip joint, with strong capsule and ligaments, does not permit discrimination of the articular cartilage of the femoral head from the acetabulum. To allow separation of acetabular and femoral cartilages in MR images, the original continuous leg traction technique was used during MR imaging [8]. However, in many cases, the joint space between the femoral cartilage and acetabular cartilage is narrow despite traction. In a related study, in case two tubular structures are close to each other, Krissian et al., analyzed the cause of its influence on centerline detection of tubular structures [9]. Therefore, for the two articular cartilages of the hip joint, it is imperative to investigate whether one can impose a limitation on the accuracy of thickness measurement, but no studies as of yet have assessed this limitation.

In this paper, we develop a mathematical model for two adjacent sheet structures based on the (one-dimensional) 1D signal intensity profile along the normal direction of two sheet structures separated by a small distance, and then perform numerical simulation of MR imaging and postprocessing for thickness

* Corresponding author at: School of Computer Science and Technology, Harbin Institute of Technology in Weihai, No. 2 Wenhuaxi Road, Weihai 264209, China. Tel.: +86 631 5687578; fax: +86 631 5687506.
E-mail address: yz_cheng@image.med.osaka-u.ac.jp (Y. Cheng).

0895-6111/$ – see front matter © 2007 Elsevier Ltd. All rights reserved.
doi:10.1016/j.compmedimag.2007.08.001

measurement. The thickness is defined as the distance between the two sides of the edges, which are the zero-crossings points of the second directional derivatives along the normal direction. We compare the measured thickness of a single sheet structure with that of the sheet structure influenced by the adjacent sheet structure and confirm that considerable underestimation error in thickness measurement occurred due to the influence of the adjacent sheet structure. To improve measurement accuracy, we propose a new measurement technique based on matching a modeled intensity profile with an actual intensity profile observed in the MR data set. Using the phantoms and two cadaveric human hip joints, we present results showing that the influence of the adjacent sheet structure is eliminated, and the improved technique is more accurate than the conventional zero-crossings method in measuring the thickness of two adjacent sheet structures.

2. Methods and materials

2.1. Theoretical simulation studies

2.1.1. Mathematical model definition

Let Sheet_1 and Sheet_2 represent the two adjacent sheet structures, which model the two cartilages in the hip joint. Fig. 1a shows a 2D representation of two adjacent sheet structures on the x–y plane. In this study, our investigations will focus on assessing the influence of Sheet_1 on thickness measurement of Sheet_2 in two dimensions (on the x–y plane). In Fig. 1a, the in-plane rotation angle θ is defined as the angle formed by the x-axis and the sheet normal direction $\vec{r}_\theta$, where $\vec{r}_\theta = (\cos\theta, \sin\theta)$. The 1D profile of the ideal density distributions of two adjacent sheets, along the x-axis (normal direction of sheet surface), can be expressed as

$$P_n(x;\tau_1,\tau_0,\tau_2) = \begin{cases} D_b, & x < -\tau_1 - \tau_0/2 \\ D_t, & -\tau_1 - \tau_0/2 \le x \le -\tau_0/2 \\ D_0, & -\tau_0/2 < x < \tau_0/2 \\ D_t, & \tau_0/2 \le x \le \tau_0/2 + \tau_2 \\ D_b, & x > \tau_0/2 + \tau_2 \end{cases}, \quad (1)$$

and two adjacent sheets perpendicular to the x-axis, can be modeled as:

$$S_0(X;\tau_1,\tau_0,\tau_2) = P_n(x;\tau_1,\tau_0,\tau_2). \quad (2)$$

where $X=(x,y)^T$, τ_0, τ_1 and τ_2 represent the distance between two adjacent sheets, Sheet_1 thickness and Sheet_2 thickness, respectively. D_b, D_t and D_0 denote the density distributions of the background of both sides, two adjacent sheets and the space between them, respectively (Fig. 1b). Two adjacent sheets with direction $\vec{r}_\theta$ can be written as:

$$S(X;\tau_1,\tau_0,\tau_2,\vec{r}_\theta) = S_0(X';\tau_1,\tau_0,\tau_2), \quad (3)$$

and

$$X' = R_\theta X. \quad (4)$$

where R_θ denotes a 2×2 matrix representing rotation θ around the z-axis.

2.1.2. MR imaging model generation

The spatial resolution of MR system can be characterized by 2D point spread function (PSF). The MR imaging of two adjacent sheets are given by

$$I_{\text{model}}(X;\tau_1,\tau_0,\tau_2,) = S(X;\tau_1,\tau_0,\tau_2,\vec{r}_\theta) \otimes \text{PSF}(X;\Delta_x,\Delta_y), \quad (5)$$

where $I_{\text{model}}(X;\tau_1,\tau_0,\tau_2)$ is the MR imaging of two adjacent sheets, $\otimes$ denotes the convolution operation. Δ_x and Δ_y represent sampling intervals along the x- and y-axis, respectively. The 2D point spread function PSF $(X;\Delta_x,\Delta_y)$ can be represented by

$$\text{PSF}(x;\Delta_x,\Delta_y) = \text{PSF}(x;\Delta_x)\text{PSF}(y;\Delta_y), \quad (6)$$

The 1D point spread function PSF $(x;\Delta_x)$ along the x-axis, is defined as follows [10]:

$$\text{PSF}(x;\Delta_x) = \frac{1}{N_x}\frac{\sin\left(\pi\frac{x}{\Delta_x}\right)}{\sin\left(\pi\frac{x}{N_x\Delta_x}\right)}, \quad (7)$$

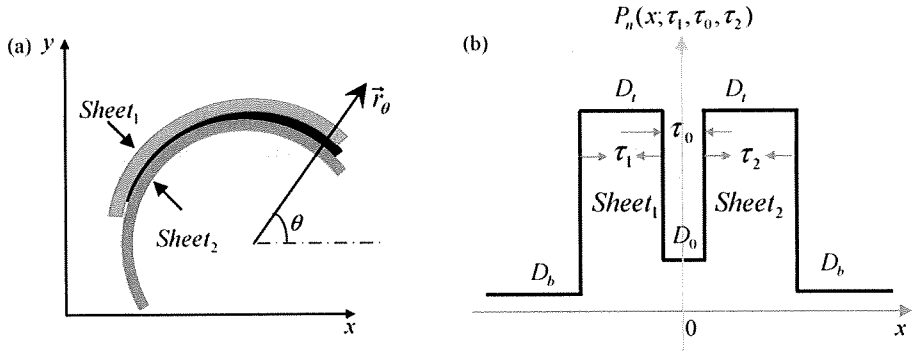

Fig. 1. The ideal model of two adjacent sheet structures. (a) 2D representation of two adjacent sheet structures. Sheet_1 and Sheet_2 represent the acetabular and femoral cartilages, respectively. The normal direction of the sheet surface is expressed as $\vec{r}_\theta = (\cos\theta, \sin\theta)$, where θ is the in-plane rotation angle. (b) 1D profile of ideal intensity distributions along the normal orientation of sheet surface for two adjacent sheets. τ_1, τ_2 and τ_0 are Sheet_1 thickness, Sheet_2 thickness and distance between them, respectively. D_b, D_t and D_0 denote the ideal intensity of the background of both sides, that of the two adjacent sheets and that of the region between them, respectively.

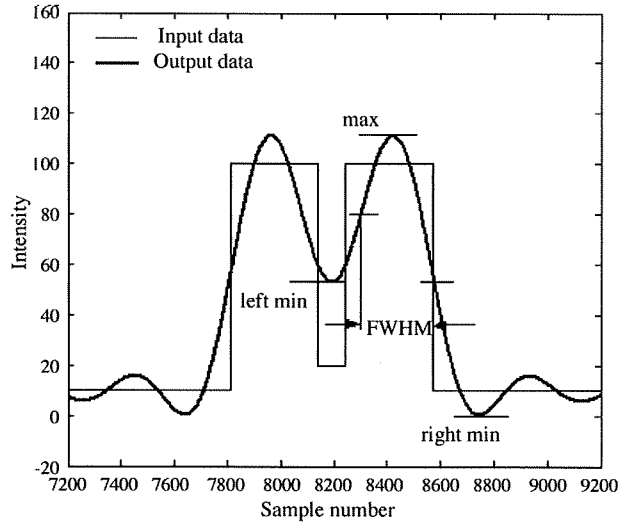

Fig. 2. 1D profile of ideal density values (input data) and MR intensity values (output data) along the normal direction, with the spatial resolution of $\Delta_x = \Delta_y = 0.625$. Note that FWHM method underestimated the thickness of Sheet_2.

where N_x is the number of samples in the frequency domain. Eq. (7) is well-approximated by

$$\text{PSF}(x; \Delta_x) = \frac{1}{N_x} \frac{\sin\left(\pi \frac{x}{\Delta_x}\right)}{\pi \frac{x}{\Delta_x}}. \tag{8}$$

2.1.3. Distribution of MR intensity at the normal line

The effects of MR imaging and limited in-plane resolution can be elucidated by analyzing 1D profile of MR intensity values, $I_{\text{model}}(X; \tau_1, \tau_0, \tau_2)$, along the normal direction θ. We assume that a parameter s denotes the position on the straight line, given by

$$X = s \cdot \vec{r}_\theta. \tag{9}$$

Thus, by substituting Eq. (9) for X in $I_{\text{model}}(X; \tau_1, \tau_0, \tau_2)$

$$I_{\text{model}}(s; \tau_1, \tau_0, \tau_2) = I_{\text{model}}(s \cdot \vec{r}_\theta; \tau_1, \tau_0, \tau_2) \tag{10}$$

is derived. Fig. 2 shows 1D profiles of the density values (input data) $P_n(x; \tau_1, \tau_0, \tau_2)$ and MR intensity values (output data) $I_{\text{model}}(s; \tau_1, \tau_0, \tau_2)$ at the normal direction $\theta = 0°$.

To explain the influence of Sheet_1 on the accuracy in thickness measurement of Sheet_2, we exhibit a profile of full-width-half-maximum (FWHM) [11–13] filter responses besides a profile of the second derivative responses described in the following Section 2.1.4. FWHM calculates a "half height point" on the left and right sides of the initial determined mid-point of profile. On each side, the minimum and maximum intensity values are calculated, and the "half height point" is located where the profile crosses the mid-point in intensity between the minimum and maximum. FWHM estimation of the profile width is defined as the distance between these half height points (Fig. 2).

2.1.4. Procedure for thickness measurement by zero-crossings method

To illustrate the potential measurement errors when applying the zero-crossings method for two adjacent sheets, we measure the thickness of Sheet_2 using the zero-crossings method. The measured thickness is defined as the distance between the left and right sides of image edges, which are the zero-crossings of second directional derivatives combined with Gaussian blurring along the normal orientation of the sheet structure. In actual situations, Gaussian blurring is employed to reduce the effect of noise. In this study, we employ a 2D Hessian matrix-based filter to enhance the boundaries of the sheet structure $I_{\text{model}}(X; \tau_1, \tau_0, \tau_2)$. Assume that $\nabla^2 I_{\text{model}}(X; \tau_1, \tau_0, \tau_2, \sigma)$ is a Hessian matrix of $I_{\text{model}}(X; \tau_1, \tau_0, \tau_2, \sigma)$ blurred by isotropic Gaussian function with a standard deviation σ, which can be written as:

$$\nabla^2 I_{\text{model}}(X; \tau_1, \tau_0, \tau_2, \sigma) = \begin{bmatrix} \frac{\partial^2}{\partial x^2} I_{\text{model}}(X; \tau_1, \tau_0, \tau_2, \sigma) & \frac{\partial^2}{\partial x \partial y} I_{\text{model}}(X; \tau_1, \tau_0, \tau_2, \sigma) \\ \frac{\partial^2}{\partial y \partial x} I_{\text{model}}(X; \tau_1, \tau_0, \tau_2, \sigma) & \frac{\partial^2}{\partial y^2} I_{\text{model}}(X; \tau_1, \tau_0, \tau_2, \sigma) \end{bmatrix}. \tag{11}$$

The second directional derivative along the normal direction of the sheet structure with respect to the image $I_{\text{model}}(X; \tau_1, \tau_0, \tau_2, \sigma)$, is given by

$$I''_{\text{model}}(X; \tau_1, \tau_0, \tau_2, \sigma, \vec{r}_\theta) = \vec{r}_\theta^{\,T} \nabla^2 I_{\text{model}}(X; \tau_1, \tau_0, \tau_2, \sigma) \vec{r}_\theta. \tag{12}$$

Similarly, the directional first derivative along the normal direction of the sheet is given by

$$I'_{\text{model}}(X; \tau_1, \tau_0, \tau_2, \sigma, \vec{r}_\theta) = \vec{r}_\theta^{\,T} \nabla I_{\text{model}}(X; \tau_1, \tau_0, \tau_2, \sigma), \tag{13}$$

in which $\nabla I_{\text{model}}(X; \tau_1, \tau_0, \tau_2, \sigma)$ is the gradient vector given by

$$\nabla I_{\text{model}}(X; \tau_1, \tau_0, \tau_2, \sigma) = (I'_{\text{model}_x}(X; \tau_1, \tau_0, \tau_2, \sigma), I'_{\text{model}_y}(X; \tau_1, \tau_0, \tau_2, \sigma)). \tag{14}$$

Thickness measurement of the sheet structure can be performed only through analyzing the 1D profile of the second directional derivative $I''_{\text{model}}(X; \tau_1, \tau_0, \tau_2, \sigma, \vec{r}_\theta)$ along the straight line. By substituting Eq. (9) for X in $I''_{\text{model}}(X; \tau_1, \tau_0, \tau_2, \sigma, \vec{r}_\theta)$, the second directional derivative along the line can be written as:

$$I''_{\text{model}}(s; \tau_1, \tau_0, \tau_2, \sigma) = I''_{\text{model}}(s \cdot \vec{r}_\theta; \tau_1, \tau_0, \tau_2, \sigma, \vec{r}_\theta). \tag{15}$$

Similarly, the first derivative along the line can be written as:

$$I'_{\text{model}}(s; \tau_1, \tau_0, \tau_2, \sigma) = I'_{\text{model}}(s \cdot \vec{r}_\theta; \tau_1, \tau_0, \tau_2, \sigma, \vec{r}_\theta). \tag{16}$$

Fig. 3a shows the 1D profiles of the second derivative responses and thickness determination procedure using a zero-crossings method for the two adjacent sheet structures. We get zero-crossing points $s = q$ and $s = p$ on the left and right sides of the edges for Sheet_2, by solving $I''_{\text{model}}(s; \tau_1, \tau_0, \tau_2, \sigma) = 0$ (shown in Fig. 3a). Let Zero-crossing

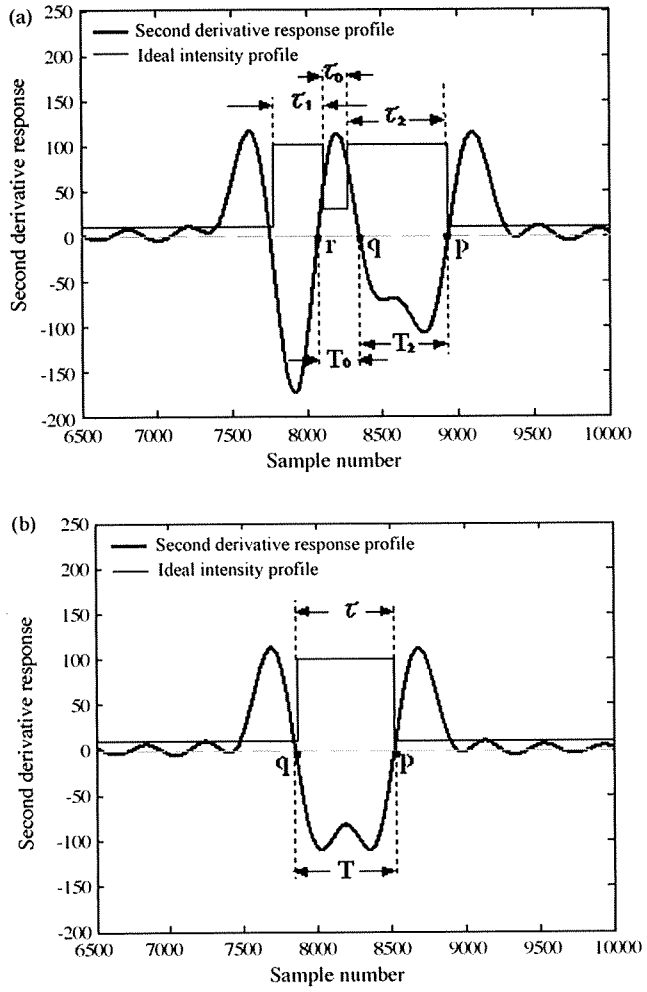

Fig. 3. Measured thickness of the sheet structures using zero-crossings method. The in-plane resolution: $\Delta_x = \Delta_y = 0.625$; Gaussian standard deviation: $\sigma = (1/2)\Delta_{xy}$ ($\Delta_{xy} = 0.625$ mm). $\tau_1 = 1.5$ mm, $\tau_0 = 0.5$ mm, $\tau_2 = \tau = 2.0$ mm. (a) Two adjacent sheets. Measured thickness of Sheet$_2$: $T_2 = |p - q|$. In the case of $\tau_0 = 0.5$ mm, thickness of $\tau_2 = 2.0$ mm was measured by approximately 1.76 mm (−12% error). Thickness of Sheet$_2$ was underestimated. (b) Single sheet. Measured thickness: $T = |p - q|$. Thickness of $\tau = 2.0$ mm was measured by approximately 2.05 mm (2.5% error).

points q and p correspond to the minimum and maximum values of $I'_{\text{model}}(s; \tau_1, \tau_0, \tau_2, \sigma)$ among those satisfying the condition given by $I''_{\text{model}}(s; \tau_1, \tau_0, \tau_2, \sigma) = 0$. The measured thickness, T_2, of Sheet$_2$ is defined as the distance between p and q, as follows:

$$T_2 = |p - q|. \tag{17}$$

In Fig. 3a, with $\tau_1 = 1.5$ mm, $\tau_0 = 0.5$ mm and $\tau_2 = 2.0$ mm, the true thickness $\tau_1 = 2.0$ mm is measured to be approximately 1.76 mm (−12% error). Fig. 3b shows the measured thickness of a single sheet. In Fig. 3b, the true thickness $\tau = 2.0$ mm is measured to be approximately 2.05 mm (2.5% error). Comparing Fig. 3a with Fig. 3b, it can be seen that measured thickness of Sheet$_2$ is underestimated as comparison with that of a single sheet.

2.2. Sample preparation and imaging

In the first experiment we imaged the four acrylic plate phantoms of sheet-like objects with known thickness. One was for a single sheet, the other three were used for two adjacent sheets with three different intervals of $\tau_0 = 0.5$, 1.0 and 1.5 mm, respectively.

(1) Single acrylic plate: Composed of four acrylic plates of 80 mm × 80 mm with true thickness $\tau = 2.0$, 1.0, 1.5, and 3.0 mm, placed parallel to each other with an interval of 30 mm (Fig. 4a).
(2) Two adjacent acrylic plates: each of the three phantoms consists of four pairs of acrylic plates, placed parallel with each other. Two adjacent acrylic plates thicknesses and the interval between them are given as follows:
   - Two adjacent sheets with τ_0 (interval between Sheet$_1$ and Sheet$_2$) = 1 mm: τ_2 (Sheet$_2$ thickness) = 2 mm, $\tau_0 = 1$ mm and τ_1 (Sheet$_1$ thickness) = 1.5 mm; $\tau_2 = 1$ mm, $\tau_0 = 1$ mm and $\tau_1 = 1.5$ mm; $\tau_2 = 1.5$ mm, $\tau_0 = 1$ mm and $\tau_1 = 1.5$ mm; $\tau_1 = 1.5$ mm, $\tau_0 = 1$ mm and $\tau_2 = 3$ mm (see from the top in Fig. 4b).
   - Two adjacent sheets with $\tau_0 = 0.5$ mm: $\tau_2 = 2$ mm, $\tau_0 = 0.5$ mm and $\tau_1 = 1.5$ mm; $\tau_2 = 1$ mm, $\tau_0 = 0.5$ mm and $\tau_1 = 1.5$ mm; $\tau_2 = 1.5$ mm, $\tau_0 = 0.5$ mm and $\tau_1 = 1.5$ mm; $\tau_1 = 1.5$ mm, $\tau_0 = 0.5$ mm and $\tau_2 = 3$ mm (not shown).
   - Two adjacent sheets with $\tau_0 = 1.5$ mm: $\tau_2 = 2$ mm, $\tau_0 = 1.5$ mm and $\tau_1 = 1.5$ mm; $\tau_2 = 1.0$ mm, $\tau_0 = 1.5$ mm and $\tau_1 = 1.5$ mm; $\tau_2 = 1.5$ mm, $\tau_0 = 1.5$ mm and $\tau_1 = 1.5$ mm; $\tau_1 = 1.5$ mm, $\tau_0 = 0.5$ mm and $\tau_2 = 3$ mm (not shown).

In the second experiment we imaged the two normal fresh-frozen cadaver hip joints (Fig. 5). After making bony defects artificially in the pelvis and the femur for landmarks, MR imaging was conducted in coronal direction with reference to the landmarks. After MR imaging, in order to obtain the anatomical thickness (See [6,14] for the detailed procedure of anatomical measurement), the hip joint was sectioned into halves, assuming an exact correlation to the imaging plane from the position of the landmarks.

MR imaging was performed with fat-suppressed 3D fast spoiled gradient-echo (SPGR) sequence on a 1.5 T MR system (Horizon, General Electric). A unilateral surface coil (TORSO, General Electric, Milwaukee, WI) was used. Four phantoms were scanned at two different in-plane rotation angles of $\theta = 0°$ and 30°. Each phantom was imaged in the sagittal plane; repetition time (TR)/echo time (TE) = 12.8/5.6 ms; flip angle = 5°; filed of view (FOV) = 160 mm × 160 mm; matrix = 256 × 256; section thickness = 1.5 mm; number of signals acquired = 2; acquisition time = 6 min 34 s. Two cadaveric hips were imaged in the coronal plane; TR/TE = 24.4/5.7 ms; flip angle = 20°; FOV = 160 mm × 160 mm; matrix = 256 × 256; section thickness = 1.5 mm; number of signals acquired = 2; acquisition time = 10 min 17 s.

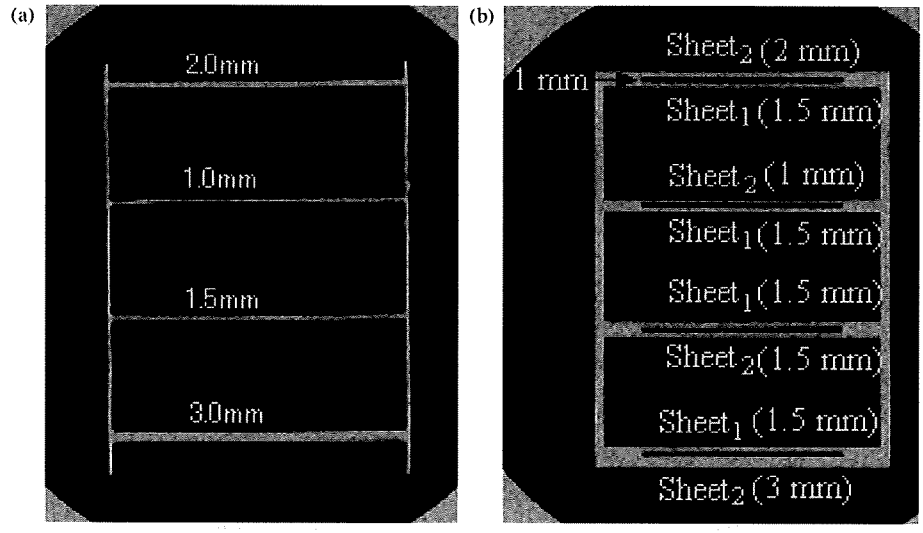

Fig. 4. MR images of acrylic plate phantoms. The horizontal and vertical axes of the images correspond to the y- and x-axis, respectively. (a) Single acrylic plate at an in-plane rotation angle of $\theta = 0°$. Thickness of Sheet_1 is 1.5 mm (not shown), and thickness of Sheet_2 is shown.

2.3. Actual thickness determination by zero-crossings method

Zero-crossings method was evaluated by using phantoms and cadaveric human hip joints. The postprocessing procedures for thickness measurement are given below. See Fig. 6 for a complete overview of thickness measurement.

2.3.1. Interpolation

In order to improve the in-plane resolution, we apply interpolation along the x- and y-directions. There are various alternative interpolation methods, but only sinc interpolation [15,16] guarantees the recovery of original information. In this experiment, sinc interpolation is used along the x- and y-directions to make the image matrix size double in the frequency domain. The sampling interval in the interpolated data is 0.3125 ($= \Delta = (1/2)\Delta_{xy}$) mm in the x-, and y-directions.

2.3.2. Extraction of sheet structure

In the actual images, it is necessary to extract the initial sheet regions before thickness determination. Using an automated segmentation technique [17,18], the approximated segmented regions of the sheets are extracted.

2.3.3. Thickness determination

For the extracted sheet structure, the boundaries of sheet structure surface are enhanced using Hessian matrix filter. This image filtering is based on the generally acknowledged theory that an edge corresponded to an abrupt change in image function, and that the first derivative should have an extreme and the

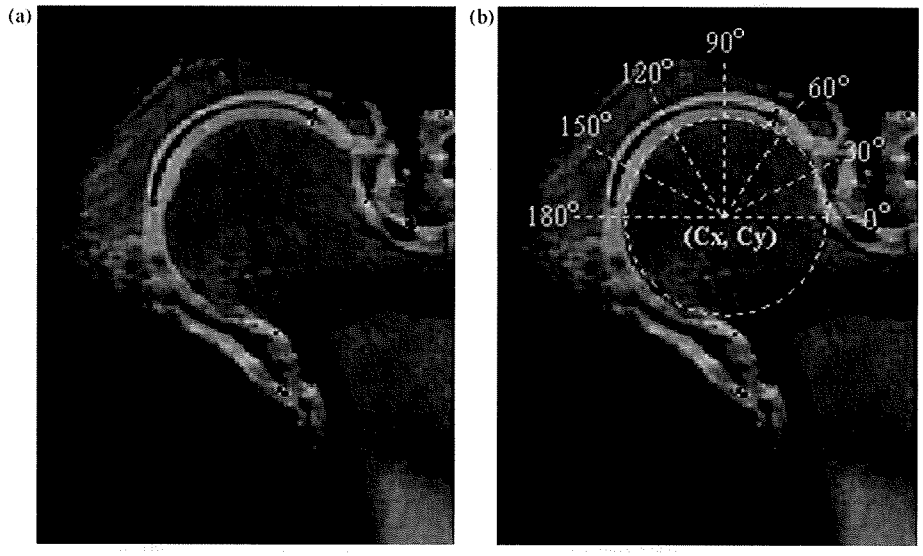

Fig. 5. Coronal MR images of a cadaver hip joint. (a) Original image. The femoral cartilage (arrowhead) is close to the acetabular cartilage (arrow). (b) Circle fitting method was employed to find the center (C_x, C_y) of the femoral head, and solid lines were drawn from this center.

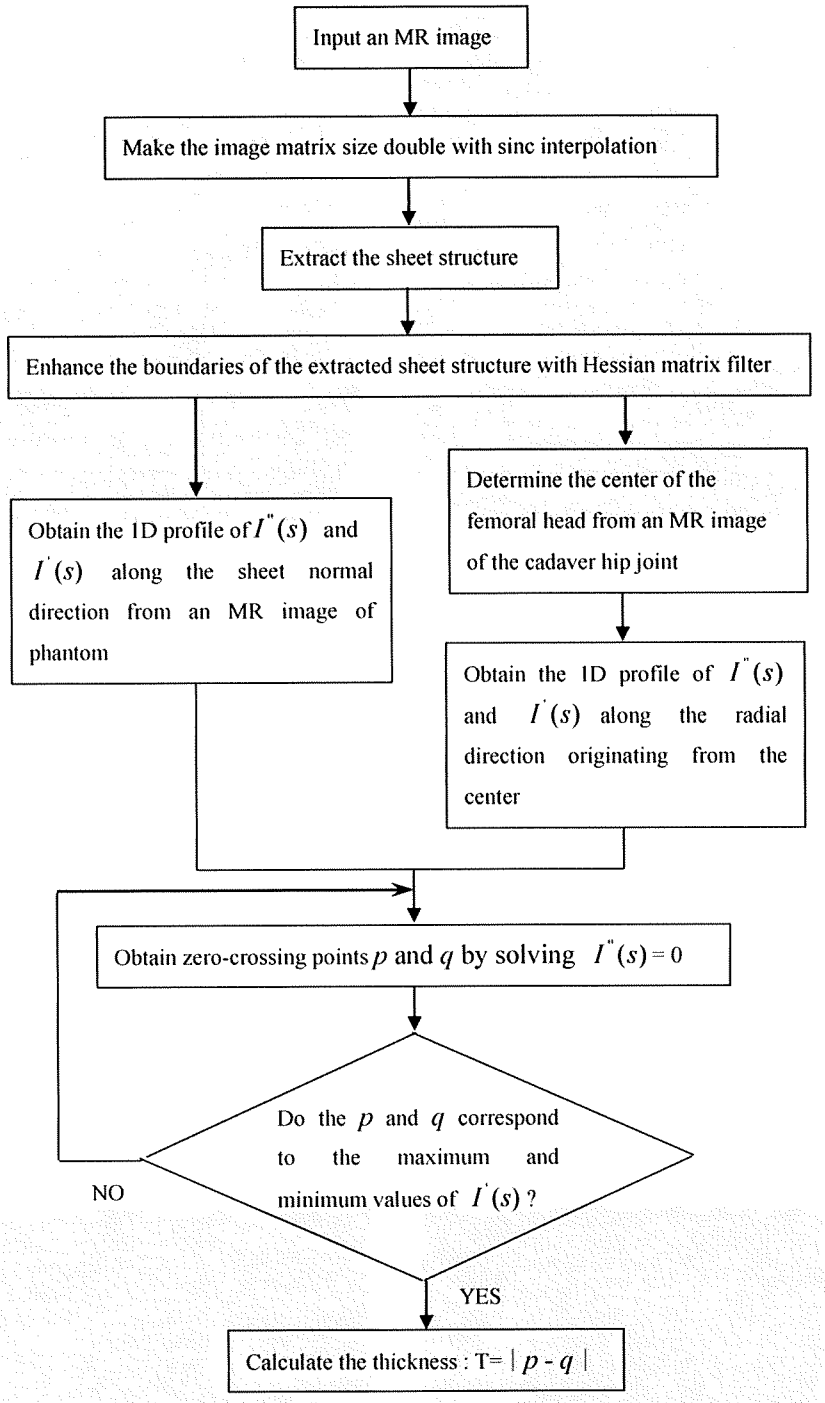

Fig. 6. Flow chart illustrating step for measuring the thickness of sheet structure using zero-crossings method.

second derivate should be equal to zero at the position of the edge.

In the experiments using the acrylic plate phantoms, the 1D profiles of the first directional derivative $I'(s)$ and the second directional derivative $I''(s)$ are obtained along the normal direction of sheet structure (acrylic plate). In the experiments using the hip joints (Fig. 5a), a circle fitting method is employed to find the center (C_x, C_y) using the boundaries of the femoral head (Fig. 5b). The 1D profiles of $I'(s)$ and $I''(s)$ are obtained along the radial direction originating from the center. Similar to Section 2.1.4, we get zero-crossing points $s = q$ and $s = p$ on the left and right sides of the edges for the sheet structure by solving $I''(s) = 0$. Let Zero-crossing points q and p correspond to the minimum and maximum values of $I'(s)$ among those satisfying the condition given by $I''(s) = 0$. The measured thickness of sheet structure is defined as the distance between p and q.

2.4. Improvement of measurement accuracy

As described in Section 2.1.4, zero-crossings method can yield large measurement errors for two adjacent sheet structures. To correct the measurement errors, we propose a new measure-

ment method based on a model of the scanning process. We model the scanning process for the two adjacent sheets and use this model to predict the shape of gray-level profiles along the sheet normal direction given in Eq. (10). The difference between the predicted profile and the actual profile observed in the MR data is minimized by refining the model parameters. The set of parameters that minimizes the difference between the model and the actual data yields the thickness estimation of the sheet structure.

We assume that D_t, D_0 and D_b are constant, while τ_1, τ_0 and τ_2 are variable at the different locations in the hip joint. We use zero-crossings method for estimating τ_1, τ_0 and τ_2. Because D_t, D_0 and D_b are constant in the entire image, if we have found one location where measured values of τ_1, τ_0, and τ_2 are regarded as a good approximation of true values τ_1, τ_0 and τ_2, D_t, D_0 and D_b at this location can be estimated accurately using this accurately measured values of τ_1, τ_0, and τ_2. In our case, when measured values of τ_1, τ_0 and τ_2 are 1.35 mm or above, these measured values can be regarded as a good approximation of their true values (this will be confirmed later in Section 3.1). If we might find several locations that satisfied the condition mentioned above, all D_t, D_0 and D_b estimated at these locations are averaged, respectively, and these average values are regarded as the estimated values of D_t, D_0 and D_b. Furthermore, τ_1, τ_0 and τ_2 at all locations are estimated accurately using D_t, D_0 and D_b obtained above, since D_t, D_0 and D_b are constant in the entire image. Briefly, the estimation procedure involves the following two steps: (1) the density values of D_t, D_0 and D_b are estimated with the accurately measured values of τ_1, τ_0 and τ_2; and 2) τ_1, τ_0 and τ_2 are estimated using D_t, D_0 and D_b estimated in the first step. See Fig. 7 for a complete overview for measuring the thickness using the improved method.

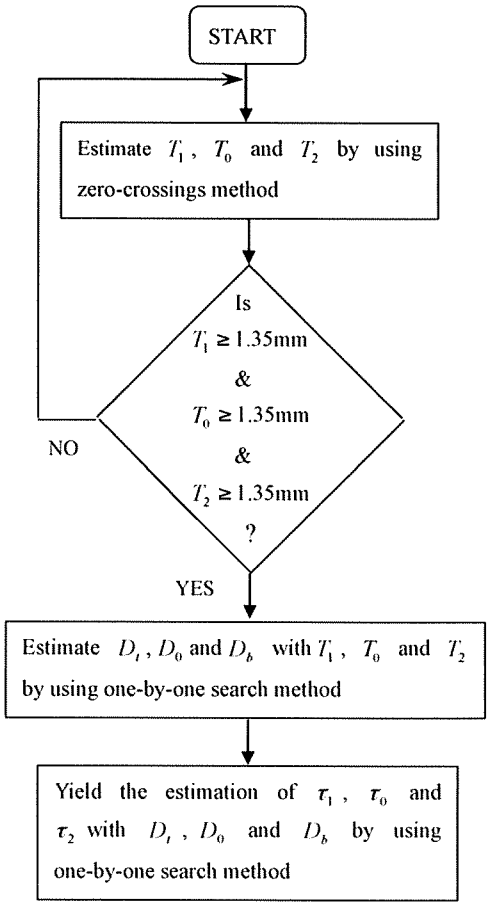

Fig. 7. Flow chart illustrating step for measuring the thickness of sheet structure using the improved method (one-by-one search method).

2.4.1. Estimation of D_t, D_0 and D_b

To estimate the density values of D_t, D_0 and D_b, the gray-level profile observed in the actual data needs to be fit to the modeled profile. Using the model of the MR imaging process, we can obtain the 1D profile of the predicted gray-level $I_{\text{model}}(s; \tau_1, \tau_0, \tau_2)$ (given in Eq. (10)) from $I_{\text{model}}(X; \tau_1, \tau_0, \tau_2)$ along the sheet normal direction $\vec{r}_\theta$. Similarly, 1D profile of the actual gray-level $I(s)$ is derived from MR image $I(X)$ along $\vec{r}_\theta$. The reconstruction of 1D profile $I(s)$ is performed at the subpixel resolution by using a bilinear interpolation.

Let T_1, T_0 and T_2 denote measured values of true values τ_1, τ_0 and τ_2, respectively, as estimated by zero-crossings method. In our case, for $T_1 \geq 1.35$ mm, $T_0 \geq 1.35$ mm and $T_2 \geq 1.35$ mm, these measured values are regarded as a good approximation of τ_1, τ_0 and τ_2. Let the observed profile be sampled at N discrete points in the actual image. With T_1, T_0 and T_2 satisfied the condition $T_1 \geq 1.35$ mm, $T_0 \geq 1.35$ mm and $T_2 \geq 1.35$ mm, D_t, D_0 and D_b are estimated by finding the values of D_t, D_0 and D_b minimizing

$$E(D_t, D_0, D_b) = \sum_{i=1}^{N} \{I(s_i) - I_{\text{model}}(s_i; T_1, T_0, T_2, D_t, D_0, D_b)\}^2. \quad (18)$$

where s_i is the ith sample along the sheet normal direction in the actual image. An optimization technique based on the Levenberg-Marquardt algorithm is used to solve this non-linear least square problem. Initial estimations of model parameters are required to start the optimization process. The initial values for D_t, D_0 and D_b are determined from the gray-level of MR image. We assume that D_t, D_0 and D_b are not locally variable and thus those are obtained as averages of all the results from the sequences of the gray-level profiles.

2.4.2. Estimation of τ_1, τ_0 and τ_2

Using estimated D_t, D_0 and D_b in the first step, τ_1, τ_0 and τ_2 are searched minimizing

$$E(\tau_1, \tau_0, \tau_2) = \sum_{i=1}^{N} \{I(s_i) - I_{\text{model}}(s_i; \tau_1, \tau_0, \tau_2, D_t, D_0, D_b)\}^2. \quad (19)$$

One drawback for Levenberg-Marquardt algorithm is the fact that the initial values of the model parameters are required to start the optimization process, and using the poor initial values can give rise to large estimation biases. As shown in Fig. 3a, the zero-crossings method exhibited considerable estimation biases for the two adjacent structures. To this end, the one-by-one search (exhaustive combination search) method is used for minimize

Eq. (19). In this study, τ_1 and τ_2 are discretized from 0.5Δ to 30Δ with 0.02Δ fixed interval ($\Delta = 0.3125$ mm), respectively, and τ_0 is discretized from 0.2Δ to 10Δ with 0.02Δ fixed interval. For all the combinations of discretized model parameters τ_1, τ_0 and τ_2, using the estimated D_t, D_0 and D_b in the first step, the cost function $E(\tau_1, \tau_0, \tau_2)$ given in Eq. (19) is calculated. Among all the combinations of the model parameters τ_1, τ_0 and τ_2, one combination of discretized model parameters τ_1, τ_0 and τ_2 corresponding to minimum value of cost function $E(\tau_1, \tau_0, \tau_2)$ is regarded as the estimations of τ_1, τ_0 and τ_2.

3. Experimental results

3.1. Measurement accuracy of zero-crossings method

3.1.1. Simulation and phantom measurements

Theoretical simulations confirm and explain that Sheet_1 affects the accuracy in the measured thickness of Sheet_2. To validate the theoretical simulations, we compare the simulated thickness with the average of actually measured thickness determined from MR images of acrylic phantoms. We also compare the measured thickness of Sheet_2 with that of a single sheet, assuming that the true thickness τ of a single sheet is the same as the true thickness τ_2 of Sheet_2. In the simulations, we mainly used the following parameters if not specified:

- True thickness of the sheet structures
  - * Two adjacent sheets: τ_1 (Sheet_1) = 1.5 mm, τ_2 (Sheet_2) = 0.5–3.0 mm.
  - * Single sheet: $\tau = \tau_2 = 0.5$–3.0 mm.
- Interval between two adjacent sheets: $\tau_0 = 0.25$–2.0 mm.
- Density values
  - * Two adjacent sheets: $D_t = 100$, $D_0 = 10$, $D_b = 0$.*Single sheet: D_5 (density value of sheet object) = 100, D_+ (density value of left-side background) = D_- (density value of right-side background) = 0.
- MR images resolution (square pixel): $\Delta_x = \Delta_y (= \Delta_{xy}) = 0.625$ mm.
- Guassian standard deviation: $\sigma = (1/2)\Delta_{xy}$.

Fig. 8 shows the results of simulation and phantom measurements. When the measured thickness values of a single sheet structure were 1.3 mm or above, these measured values could be regarded as a good approximation of their true thickness. Compared with the measured thickness of a single sheet structure, thickness of sheet structure influenced by adjacent sheet structure was considerably underestimated (Fig. 8a). The degree of underestimation of thickness was determined with the distance between the two adjacent sheet structures being less than 1.3 mm. The error between the simulated thickness and the average of actually measured thickness with phantoms of two adjacent sheets was smaller than 0.1 mm, and S.D. of actually measured thickness was within 0.1 mm (Fig. 8b). We also compared simulated thickness with the average of actually measured thickness with phantom of a single sheet. A good agreement between the simulation and phantom measurements was also observed (not shown). The numerical simulation

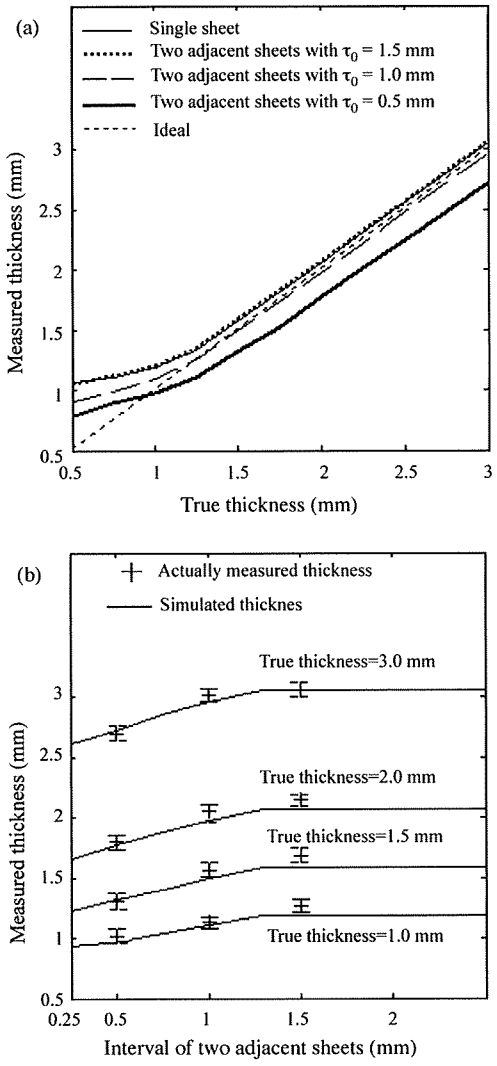

Fig. 8. Numerical simulation and phantom measurements with zero-crossings method. Gaussian standard deviation $\sigma = (1/2)\Delta_{xy}$ ($\Delta_{xy} = 0.625$ mm) and MR images of phantoms at $\theta = 0°$ were used. (a) Relationship between the measured thickness and the true thickness with simulation measurements. (b) Relationship between the measured thickness and the true interval of the two sheets. The measured thickness T_2 (average ± S.D.; $n = 50$) of phantoms also was shown. The error between the simulated thickness and the average of the actually measured thickness with phantoms was lower than 0.1 mm, and S.D. of the actually measured thickness was within 0.1 mm. The simulation was validated by phantom measurement.

was validated by experiments using actual MR images of phantoms.

Fig. 9 shows the relationship between the true interval τ_0 and the measured interval T_0 with a zero-crossings method. In Fig. 9, in the case of $\tau_1 = 1.5$ mm and $\tau_2 = 1.0$ mm, the interval between two sheets was measured. A good agreement between the simulated and the actually measured intervals was shown in Fig. 9. The results of Fig. 9 show that for measured interval value $T_0 \geq 1.3$ mm, these measured values were approximately equivalent to the true interval τ_0. Similarly, using $\tau_1 = 1.5$ mm and $\tau_2 = 1.5, 2.0$, and 3.0 mm, comparisons between τ_0 and T_0 were performed. The same results as Fig. 9 were observed.

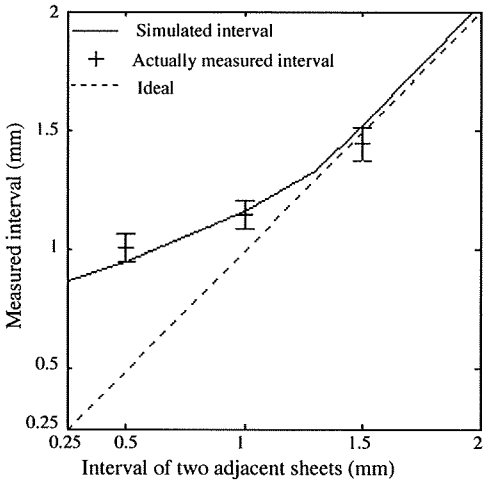

Fig. 9. Relation between the true interval τ_0 and the measured interval T_0 (average ± S.D.; $n = 50$) using a zero-crossings method. Guassian standard deviation $\sigma = (1/2)\Delta_{xy}$ ($\Delta_{xy} = 0.625$ mm) and MR images of a phantom at $\theta = 0°$ were used. Graph shows that for $T_0 \geq 1.3$ mm, these measured values are a good approximation of their true interval.

3.1.2. Measurements of cartilage thickness and joint space width

To specify how cartilage thickness and joint space width can be accurately measured by using zero-crossings method, we selected 10 positions in the anatomical section and in MR images, ranging from 135° to 150° (Fig. 5b) and performed the comparison of anatomic measurement and zero-crossings measurement (Table 1). The values of the examined 10 positions averaged $\tau_2 = 1.35 \pm 0.04$ mm at the anatomical sections and $T_2 = 1.36 \pm 0.08$ mm in an MR image for femoral cartilage thickness, $\tau_1 = 2.63 \pm 0.09$ mm at the anatomical sections and $T_1 = 2.56 \pm 0.12$ mm in an MR image for acetabular cartilage thickness, and $\tau_0 = 1.32 \pm 0.03$ mm at the anatomical sections and $T_0 = 1.36 \pm 0.06$ mm in an MR image for joint space width, respectively. From the experimental results we concluded that for the measured values of 1.35 mm or above, these values could be regarded as a good approximation of their true values. This is consistent with the results predicted by the numerical simulation.

3.2. Improvement of measurement accuracy

3.2.1. Phantom measurement

Fig. 10 shows the average measurement error and standard error for the zero-crossings, the improved methods at $\theta = 0°$ (Fig. 10a) and 30° (Fig. 10b). As shown in Fig. 10a and b, in the case of $\tau_1 = 0.5$ mm, the measured thickness of Sheet_2 was influenced by Sheet_1 when using a zero-crossings method. The improved method (one-by-one search method) gave measurements with less estimation bias than zero-crossings.

3.2.2. Cartilage thickness measurement

Linear regression and correlation analyses are carried out to examine the relationships between measurements obtained with our improved method and anatomical measurements, and between measurements obtained with zero-crossings method and anatomical measurements. The slope and the intercept of regression line are analyzed to determine the degree to which the two methods produced identical results. Regression equations are compared with the equation of the line of identity using t-statistics for the slope and the intercept. Differences in method measurement accuracy are assessed using paired t-tests. $p < 0.05$ was considered as the significant level for all statistical tests.

Fig. 11 indicates the determination procedures of the improved method for measurement of femoral cartilage thickness. The thickness of femoral cartilage was measured as 2.10 mm anatomically, 1.77 mm by zero-crossings method and 2.03 mm by the improved method. For accuracy determination, anatomical measurement of femoral cartilage thickness was set as reference. The improved method exhibited smaller estimation bias than zero-crossings method.

As shown in Fig. 12a, comparison of femoral cartilage thickness estimated by the zero-crossings method with the anatomical thickness produced a regression relationship ($y = 0.91x - 0.15$) with both the slop and the intercept differing significantly from one and zero, respectively ($p < 0.01$). The improved method shows a regression relationship ($y = 1.02x - 0.03$)

Table 1
Comparison of anatomic measurement and zero-crossings measurement

Positions	Anatomic measurement (mm)			Zero-crossings measurement (mm)		
	Femoral cartilage thickness	Joint space width	Acetabular cartilage thickness	Femoral cartilage thickness	Joint space width	Acetabular cartilage thickness
1	1.38	1.30	2.63	1.29	1.43	2.57
2	1.32	1.27	2.81	1.38	1.35	2.81
3	1.30	1.32	2.75	1.17	1.45	2.77
4	1.36	1.31	2.56	1.41	1.33	2.45
5	1.29	1.31	2.54	1.39	1.39	2.48
6	1.36	1.32	2.59	1.33	1.36	2.52
7	1.31	1.36	2.62	1.41	1.35	2.53
8	1.36	1.38	2.57	1.45	1.34	2.50
9	1.37	1.35	2.65	1.42	1.30	2.51
10	1.42	1.29	2.58	1.38	1.26	2.49
Mean	1.35	1.32	2.63	1.36	1.36	2.56

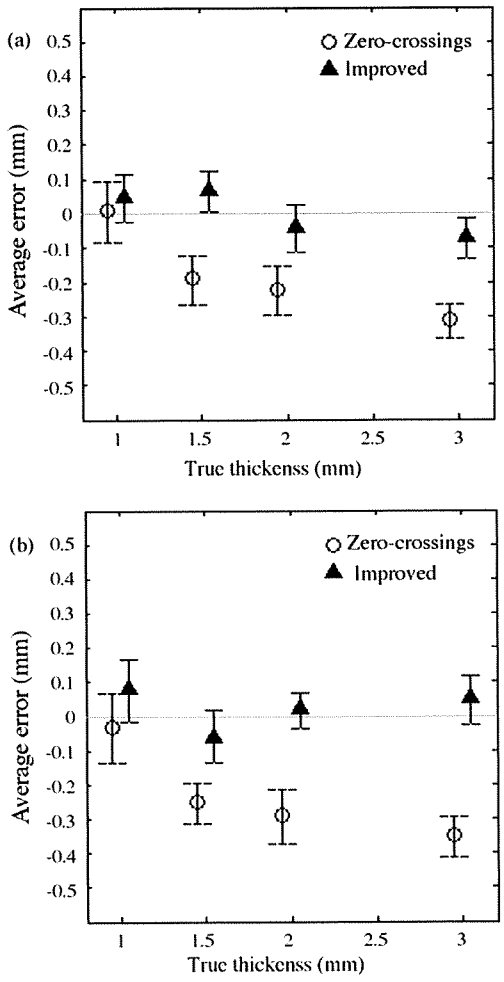

Fig. 10. Comparison of the average of measurement error (measured thickness-true thickness) obtained with the improved method to the average measurement error obtained with the zero-crossings method. Graph shows the average measurement error and standard error ($n=50$). (a) In-plane rotation $\theta=0°$. (b) In-plane rotation $\theta=30°$.

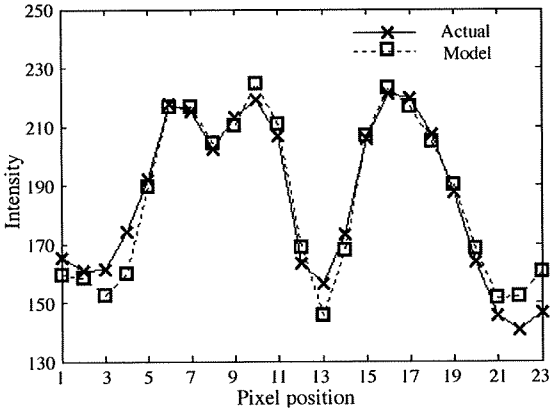

Fig. 11. Modeled gray-level profile and actual gray-level profile along the 100° radial direction (see Fig. 5b) after applying an optimization technique (one-by-one search algorithm). Femoral cartilage thickness, joint space width and acetabular cartilage thickness were estimated to be 2.10, 0.53 and 2.02 mm with the anatomical method, to be 1.77, 1.03 and 1.72 with the zero-crossings method, and to be 2.03, 0.41 and 2.15 mm with the improved method (one-by-one search algorithm).

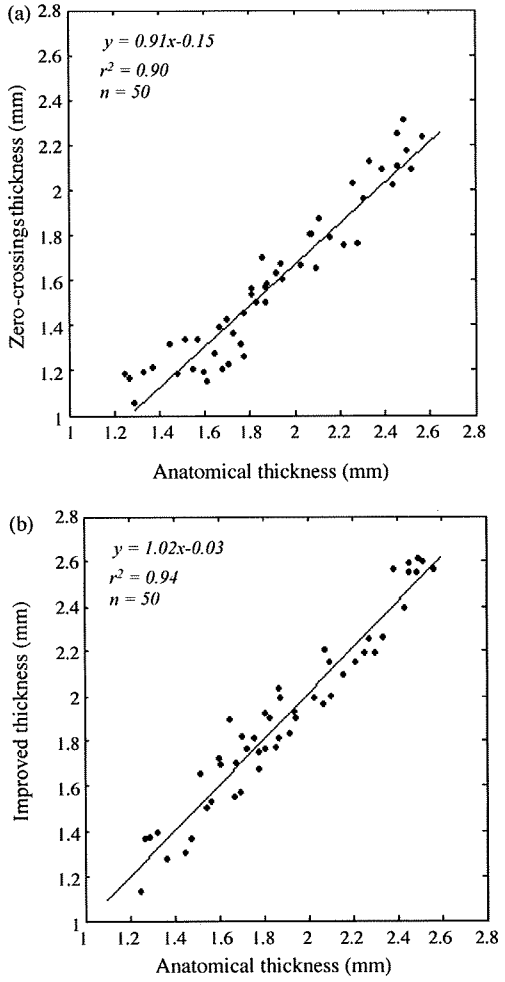

Fig. 12. Comparison of three methods for estimating the femoral cartilage thickness at the selected 50 positions with joint space width $\tau_0 < 1.25$ mm. (a) Cartilage thickness measured by zero-crossings method plotted against cartilage thickness measured by anatomic method at 50 positions. The line of best fit constructed at regression analysis and the corresponding regression equation also are shown. Linear regression analysis shows good agreement between cartilage thickness measured by zero-crossings method and that measured by anatomic method ($r_2=0.90$, $p<0.01$). However, The slope (0.91) and intercept (−0.15) of the regression line was significantly different from one and zero, respectively ($p<0.01$). The zero-crossings method underestimated the cartilage thickness in comparison to the anatomic measurement. (b) Cartilage thickness measured by the improved method plotted against cartilage thickness measured by anatomic method at 50 positions. The line of best fit constructed at regression analysis and the corresponding regression equation also are shown. Linear regression analysis yielded $r^2=0.94$, the slope and intercept of the regression line being 1.02 and −0.03, respectively. This shows that there is not only a strong linear relationship between the two measurements, but also very good agreement between the values obtained with both methods. A paired t-test shows the differences between the improved measurement from MR images and anatomic measurement is not statistically significant ($p>0.1$).

closely approximating the line of identity with neither the slope nor the intercept (Fig. 12b). The anatomical measurement of cartilage thickness was used as the reference with which those obtained by the zero-crossings and improved measurements were compared. The results indicated that femoral cartilage thickness estimated using the improved method was significantly more accurate than that estimated by the zero-crossings method ($p<0.01$). Fig. 13a shows the difference

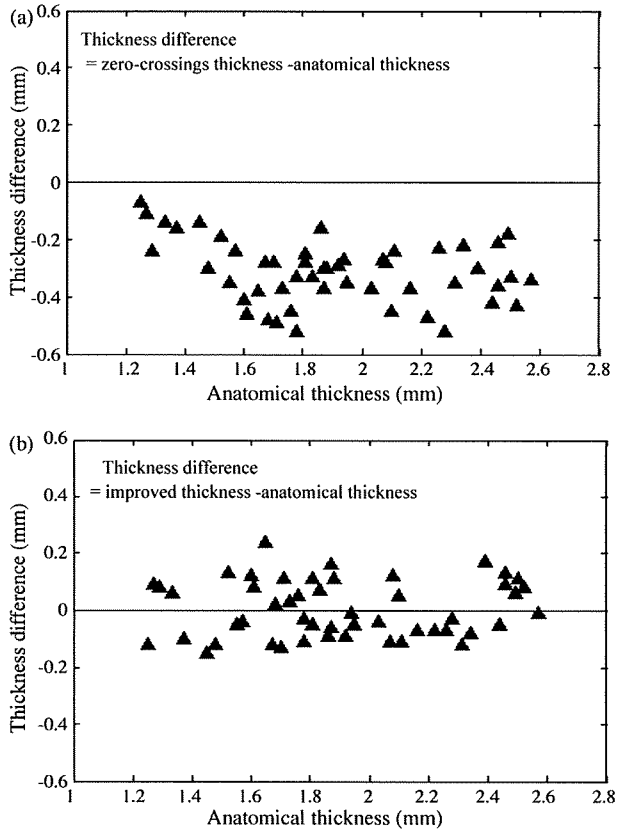

Fig. 13. Difference in the measured thickness between the methods. (a) Difference in the measured thickness between zero-crossings and anatomical methods. (b) Difference in the measured thickness between the improved and anatomical methods. The thickness of the femoral cartilage was estimated at 50 different positions along the radial direction originating from the center of the femoral head. Graph shows that the improved method gave the results similar to those presented from anatomical section, while the zero-crossings gave underestimation relative to the anatomical thickness.

in the measured thickness between the zero-crossings and anatomical methods. Fig. 13b shows the difference in the measured thickness between the improved and anatomical methods. Anatomical measurement of cartilage thickness was used as reference. The zero-crossings method gave considerable measurement bias (underestimating the cartilage thickness), while the improved method gave measurements with less estimation bias.

4. Discussion

As for two adjacent sheet structures ($Sheet_1$ and $Sheet_2$), such as femoral cartilage and acetabular cartilage in the hip joint, we performed the simulation measurement, phantom measurement and articular cartilage thickness measurement. The experimental results showed considerable underestimation in thickness measurement occurred due to the influence of the adjacent sheet structure. In order to remove the influence of the adjacent sheet and calibrate measurement bias, an improved measurement method was presented. The main findings of our work are as follows:

4.1. Observation of profiles by FWHM and zero-crossings methods

In order to clarify the cause of the influence of the adjacent sheet ($Sheet_1$) on the accuracy of thickness measurement of $Sheet_2$, we showed the profiles of thickness determination procedures using FWHM (see Fig. 2) and zero-crossings (see Fig. 3a) methods. The profiles of the two determination procedures distinctly exhibited the influence of the adjacent sheet on the accuracy of thickness measurement. Through observing the profiles produced by FWHM and zero-crossings methods, we can see that the adjacent sheet resulted in the underestimation of thickness. In this study, we further used zero-crossings method to analyze the measurement accuracy of the sheet structure thickness.

4.2. Effect of Gaussian standard deviation σ

In the actual image, Gaussian blurring is employed to remove the noise. The degree of smoothing is determined by the Gaussian standard deviation σ. Better effectiveness of Gaussian smoothing require larger the standard derivation of Gaussian. On the other hand, we should notice that larger standard derivation of Gaussian give rise to greater underestimation of thickness. In this study, we performed the thickness measurement with $\sigma = (1/2)\Delta_{xy}$, $\sigma = (\sqrt{2}/2)\Delta_{xy}$ (not shown) and $\sigma = \Delta_{xy}$ (not shown). When $\tau_0 > 3$–4σ, the accuracy of thickness measurement was not affected by the adjacent sheet. This means, the measured thickness of $Sheet_2$ was approximately the same as that of a single sheet.

4.3. The validity of the simulation

The results of phantom measurements and simulations showed that the bias between the actually measured thickness and the simulated thickness was nearly within 0.1 mm (see Fig. 8b). The validity of theoretical simulations was confirmed. Thus, we can use mathematical model of two adjacent sheets and MR imaging parameters to predict the measurement accuracy. Also, thickness measurement can be performed only through analyzing 1D profile of the second derivative responses along the normal direction of sheet surface, so the computation of the simulations is simplified and its cost is drastically reduced.

4.4. Normal direction of the cartilage surface

In the present study, two healthy cadaveric specimens of human hip were used for determining the femoral cartilage thickness. We assume that the shape of the femoral head approximates the exact sphere. Therefore, we employed a circle fitting method to find the center using the boundaries of the femoral cartilage. The radial directions from the detected center can be regarded as the normal direction of the cartilage surface. However, as in the case of diseased hip joint, because the shape of the femoral head is not perfectly spherical, this method cannot be used. In such cases, the normal direction

might be estimated using the eigenvectors of the Hessian matrix [19].

4.5. An improved measurement method

To improve the accuracy of thickness measurement, we developed a new technique based on a model of the MR imaging process for two adjacent sheet structures separated by a small distance. Thickness estimation problem is formulated as a least square fitting of an actual gray-level profile observed in the MR data set to a modeled gray-level profile. The difference between the modeled profile and the actual gray-level profile observed in the MR data is minimized by refining the model parameters. We employed an exhaustive one-by-one search algorithm to minimize this difference, not using the Levenberg-Marquardt algorithm. One drawback for Levenberg-Marquardt algorithm is the fact that the initial values of the model parameters are required to start the optimization process, and using the poor initial values can give rise to large estimation biases. The zero-crossings method exhibited considerable estimation biases for the two adjacent sheet structures (see Fig. 8). An attempt was made to obtain the initial values of τ_1, τ_0, and τ_2 using zero-crossings method. Levenberg-Marquardt algorithm yielded the poor estimations of τ_1, τ_0, and τ_2 when applying the zero-crossings method to obtain the initial values. Thus, one-by-one search method was used to minimize the difference between the modeled profile and the actual gray-level profile observed in the MR data.

Our new improved technique is not only available for two adjacent sheets but also available for a single sheet. There are inherent limitations on the accuracy in thickness measurement of a single sheet due to finite spatial resolution of imaging scanners and blurring involved in edge detections [20,21]. For two adjacent sheets, there is a limitation of the influence of the adjacent sheet, as well as those mentioned above. Our improved method can overcome these limitations. Using zero-crossings method, for the sheet structure affected by the adjacent sheet, the measured thickness value is an underestimation relative to its true thickness, whereas for the unaffected sheet with a small thickness, its measured value is an overestimation relative to its true thickness (see Fig. 8). The improved method gave the accurate measurements in both cases.

In conclusion, in this paper, we confirmed that for two adjacent sheet structures, considerable underestimation in thickness measurement occurred due to the influence of the adjacent sheet structure. A new technique based on a model of the MR imaging process was proposed to improve the measurement accuracy. In our present work, in the case of isotropic resolution, measurement accuracy analysis and improvement of accuracy were performed. In generally, the resolution of medical 3D data along z-direction (the direction perpendicular to the slice plane) is lower than within slices, this means that the voxel of 3D image is anisotropic. Therefore, in the future work, the effect of anisotropic voxel on measurement accuracy requires investigation, and then the calibration of measurement bias would be needed to perform. Finally, our work will focus on clinical validation using a large set of data for applications.

5. Summary

In the hip joint, in which the femoral and acetabular cartilages are adjacent to each other. To investigate whether the accuracy in thickness measurement of femoral cartilage is influenced by acetabular cartilage, we developed a mathematical model for two adjacent sheet structures, which simulated the femoral and acetabular cartilages in the hip joint. MR imaging process and post\processing for thickness measurement are also modeled and simulated. Thickness is defined as the distance between the two sides of the edges, which are the zero-crossing points of the second derivatives combined with Gaussian blurring along the normal direction. The result of simulation measurements shows that considerable underestimation in thickness measurement occurred due to the influence of the adjacent sheet structure. In order to remove the influence of the adjacent sheet and calibrate measurement bias, we propose a new measurement method based on a model of the MR imaging process. Using this model, we can predict the shape of the gray-level profile along the normal direction of the sheet surface. Thickness estimation problem is formulated as a least square fitting of an actual gray-level profile observed in the MR data set to a predicted gray-level profile. Using a one-by-one search (exhaustive combination search) technique, the model parameters are adjusted to minimize the differences between the predicted and the actual gray-level profiles observed in the MR data. The set of parameters that minimizes the differences yields the thickness estimation of the sheet structure. In the experiments, we imaged the acrylic plate phantoms and two normal cadaver hip joints. All MR images were acquired with a resolution of 0.625 mm × 0.625 mm × 1.5 mm. In the first experiment, we tested the accuracy of the conventional zero-crossings method using phantoms. The result of phantom measurements shows that the zero-crossings method underestimated the thickness of two adjacent sheet structures. The error between simulation measurement and phantom measurement was smaller than 0.1 mm, and S.D. of actually measured thickness was within 0.1 mm. A good agreement between the simulation and phantom measurements was observed. The numerical simulation was validated by experiments using actual MR images of phantoms. In the second experiment, we performed the comparison of the zero-crossings method and the new improved method. In the experiment using phantoms, the results show that our new improved method was more accurate than zero-crossings method. In the experiment using two cadaveric human hip joints, the results obtained by the new improved method for cartilage thickness measurement were significantly different from those generated by zero-crossings method ($p < 0.01$) and were more accurate when compared using paired t-tests. In conclusion, in this paper, we confirmed that for two adjacent sheet structures, considerable underestimation in thickness measurement occurred due to the influence of the adjacent sheet structure. Using phantoms and two normal cadaver hip joints, we present results showing that the new improved method removed the influence of the adjacent sheet and was more accurate than the conventional zero-crossings method in estimating thickness of two adjacent sheet structures.